applied sciences

MDPI

Article

Numerical Study on the Feasibility of a 24 GHz ISM-Band Doppler Radar Antenna for Near-Field Sensing of Human Respiration in Electromagnetic Aspects

Seungyong Park [1], Sungpeel Kim [1], Dong Kyoo Kim [2], Jaehoon Choi [1] and Kyung-Young Jung [1,*]

[1] Department of Electronics and Computer Engineering, Hanyang University, Seoul 04763, Korea; seungyeng@hanyang.ac.kr (S.P.); spcl1@hanyang.ac.kr (S.K.); choijh@hanyang.ac.kr (J.C.)
[2] Hyper-connected Communication Research Laboratory, Electronics and Telecommunications Research Institute, Daejeon 34129, Korea; kdk3606@etri.re.kr
* Correspondence: kyjung3@hanyang.ac.kr; Tel.: +82-2-2220-2320

Received: 10 July 2020; Accepted: 2 September 2020; Published: 4 September 2020

Abstract: The feasibility study of a 24 GHz industrial, scientific, and medical (ISM) band Doppler radar antenna in electromagnetic aspects is numerically performed for near-field sensing of human respiration. The Doppler radar antenna consists of a transmitting (Tx) antenna and a receiving (Rx) antenna close to the human body for a wearable device. The designed slot-type Doppler radar antenna is embedded between an RO4350B superstrate and an FR-4 substrate. To obtain the higher radiation pattern of the antenna towards the human body, a ground plane reflector is placed underneath the substrate. The measured −10 dB reflection coefficient (S_{11}) bandwidth is 23.74 to 25.56 GHz and the mutual coupling (S_{21}) between Tx and Rx antennas is lower than −30 dB at target frequencies. The Doppler radar performance of the proposed Doppler radar antenna is performed numerically by investigating the signal returned from the human body. The Doppler effect due to human respiration is investigated through the I/Q and arctangent demodulation of the returned signal. According to the results, the phase variation of the returned signal is proportional to the displacement of the body surface, which is about 0.8 rad in accordance with 1 mm displacement. The numerical experiments indicate that the proposed Doppler radar antenna can be used for near-field sensing of human respiration in electromagnetic aspects.

Keywords: doppler radar; slot antenna; I/Q demodulation

1. Introduction

As we rapidly become a super-aging society, the global medical device market is growing. Medical devices can improve the quality of life by providing a health status to assist a patient by diagnosing and treating the patient's health condition. The Doppler radar, in particular, has been widely used as a promising medical device for detecting vital signs [1–4]. The Doppler radar can diagnose the health condition by detecting the movement of the human body surface. If the radiofrequency (RF) signal transmitted from the Doppler radar reaches the human body, displacement due to body surface movement results in the phase shift of the returned RF signal. The phase shift of the returned signal is linearly proportional to the displacement by the Doppler effect [5,6]. Therefore, the Doppler radar can indicate cardiopulmonary function by analyzing the phase changes associated with displacement. Conventional 2.4 GHz Doppler radars have been studied for contactless applications and nowadays higher-frequency band Doppler radars are widely studied. The K-band Doppler radar can especially

provide several advantages compared to low frequency bands. It can have high sensitivity to small displacements of the human body and can be miniaturized [7–10]. Note that one of unlicensed radio bands is the 24 GHz industrial, scientific, and medical (ISM) band. However, conventional Doppler radars for sensing human vital signs are usually used in limited spaces because they are installed on fixed locations and operate remotely in the far field. Therefore, it is impossible to detect human vital signs when a person leaves a stationary test site in the conventional Doppler radar system. To overcome the limitation, the Doppler radar is necessary to be designed for wearable devices, which allows detection of human vital signs without space limitations. Note that the wearable device directly attached to the human body is not appropriate for near-field sensing of human vital signs due to zero relative displacement. The wearable device with a strap wrapping the human body (e.g., an ID badge holder or a wrist band) can be considered for near-field sensing of human vital signs, because the Doppler radar does not move in relation to the human cardiopulmonary motion or pulse. When the Doppler radar antenna is placed in the vicinity of the human body (whose electrical properties are high permittivity and conductivity at 24 GHz), the antenna performance may be degraded. In other words, the frequency response of the antenna may be distorted due to human body effects. Therefore, the Doppler radar antenna for wearable devices should be less affected by human body effects.

In this paper, we study a 24 GHz ISM-band Doppler radar antenna suitable for near-field sensing of human vital signs. As a proof of concept, we present the feasibility study of the Doppler radar antenna close to the human body to sense human respiration in the viewpoint of antennas and propagation. The Doppler radar antenna should be designed to provide good matching performance and low mutual coupling for sufficient isolation between the transmitter and the receiver [11,12]. The slot-type antenna is less affected by human body effects compared to other antennas [13]. Therefore, in this work, the slot-type Doppler radar antenna with good performance is designed and fabricated. To demonstrate the performance of the designed Doppler radar antenna, the Doppler radar antenna in front of the Duke phantom's abdomen [14] is simulated by using Sim4life [15], which is based on the finite-difference time-domain (FDTD) method [16–18]. The performance is evaluated by analyzing the signal returned from the phantom. The phase variation of the received signal is converted to displacement due to human motion by using I/Q demodulation because quadrature receivers are commonly used in Doppler radar to detect vital signs. Note that displacement can be obtained through the ratio of two I/Q channel output signals in a quadrature receiver system, which is called by the arctangent demodulation. It is found that the phase variation is linear with respect to displacement due to the Doppler effect. This work considers simulations on scenarios with body-RF signals interaction that give a qualitative insight of the feasibility of this antenna system for near-field sensing of human vital signs. Further work is necessary to validate the Doppler radar for near-field sensing of vital signs, since it will be feasible when the electromagnetic performance as well as the performance of other parameters in RF systems, baseband systems, and the underlying signal processing are fully considered. The remainder of this paper is organized as follows. We first present the design and measurement results of the slot-type Doppler radar antenna. Next, we investigate the performance of the designed Doppler radar antenna close to the human body and conduct a feasibility study of the 24 GHz ISM-band Doppler radar antenna for near-field sensing of human respiration. Finally, concluding remarks are provided.

2. Slot-Type Doppler Radar Antenna Design

As alluded previously, the slot-type Doppler radar antenna [19] is designed in this work, since slot antennas are less affected by human body effects compared to other antennas. Figure 1a shows the overall view of the designed slot-type antenna. Both Tx port (Port 1) and Rx port (Port 2) are fed by the end-launch K-connectors and they are connected to the microstrip line through via-holes. The slotted aperture is embedded between the superstrate and the substrate, which are Rogers RO4350B (thickness = 0.254 mm, ε_r = 3.48, tan δ = 0.0037) and FR-4 (thickness = 1.6 mm, ε_r = 4.4, tan δ = 0.02), as depicted Figure 1b. The FR-4 substrate is employed for rigidity because the antenna on Rogers RO4350B may be easily bent. The antenna has a slot of 0.8 × 2.8 mm^2, as shown in Figure 1c. The radiation pattern of

slot antenna is basically omnidirectional pattern. In order to obtain a higher radiation pattern towards the human body than the back side, the slot antenna has a reflector underneath the FR-4 substrate as shown in Figure 1d. Figure 2 shows the microstrip line-based feed circuit. The microstrip lines are printed on the top layer of Rogers RO4350B superstrate and ground planes with slotted aperture are mounted on bottom layer of Rogers RO4350B superstrate. The width of microstrip line is 0.5 mm and its length is 7.3 mm.

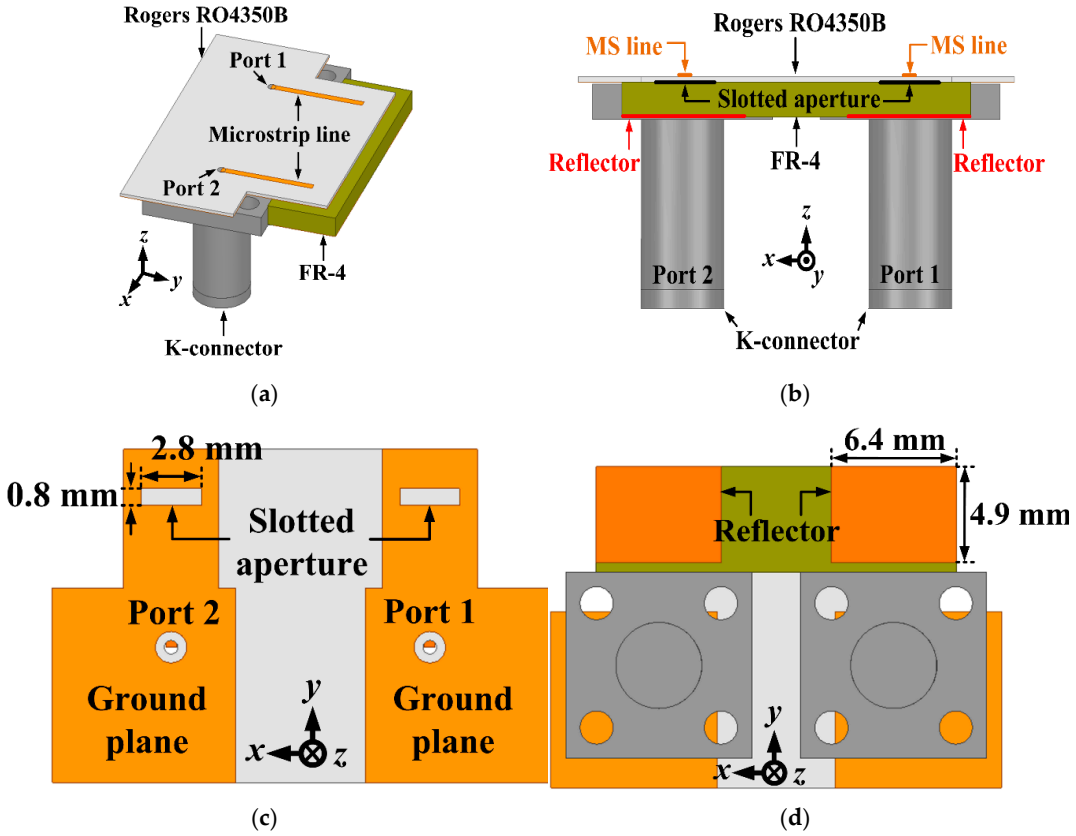

Figure 1. Designed slot-type Doppler radar antenna: (**a**) overall view; (**b**) slotted aperture; (**c**) side view; (**d**) bottom view.

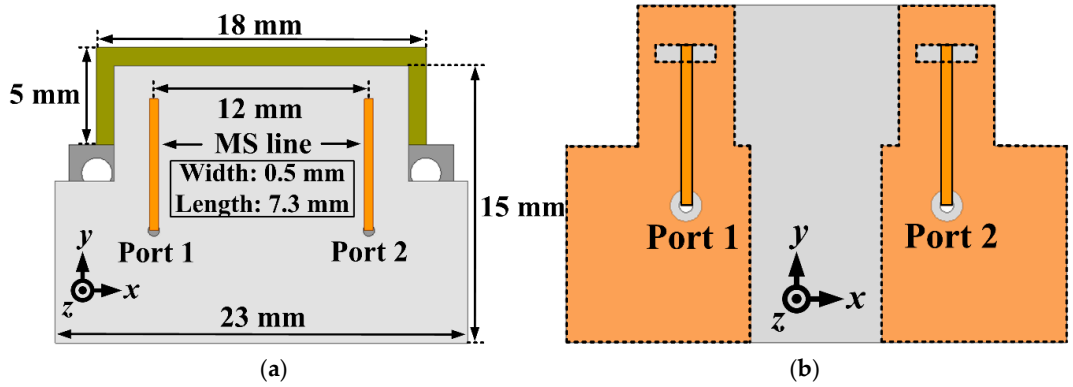

Figure 2. Feed circuit of slot-type Doppler radar antenna: (**a**) designed microstrip-line on Rogers RO4350B superstrate; (**b**) perspective view of microstrip-line and slotted aperture.

The surface current is induced around the slotted aperture by electromagnetic coupling with the microstrip line. Therefore, the slotted apertures work as a slot antenna [20]. The impedance characteristic of the slot antenna can be controlled by modifying the length and width of the microstrip line. The surface current distributions at 24.125 GHz is shown in Figure 3. The designed slot-type

Doppler radar antenna is fabricated and measured in Figure 4. As shown in Figure 4, simulation and measurement results are obtained by considering the slot-type Doppler radar antenna system composed of Tx and Rx antennas, not just only one antenna. Figure 5 shows the simulated and measured S-parameters of the Tx antenna. The simulated reflection coefficient (S_{11}) of the slot-type antennas is below −10 dB from 23.2 to 24.78 GHz (bandwidth BW = 1.58 GHz). The simulated mutual coupling (S_{21}) from the Tx antenna to the Rx antenna is lower than −27.4 dB over the target frequency band. The measured −10 dB S_{11} bandwidth is 23.74 to 25.56 GHz (BW = 1.82 GHz) and the measured S_{21} is lower than −30 dB over the target frequency band. The discrepancies between simulation and measurement are regarded as error by the manufacturing process. Although the resonant frequency is shifted to a higher band, the fabricated antenna still covers the target frequency band. The simulated and measured radiation patterns of the Tx antenna are shown in Figure 6, when port 1 is excited. The simulated realized gain and front-to-back ratio (FBR) along z-axis are 4.24 dBi and 9.23 dB, respectively. The simulated cross polarization (X-pol) level is significantly lower than the simulated co polarization in the front side. The measured realized gain and FBR along z-axis are 2.1 and 33.3 dB, respectively. The discrepancies between simulation and measurement in terms of radiation patterns are caused by the same reasons for S-parameters. It should be also noted that the radiation pattern of the designed slot-type antenna is different from that of the basic slot antenna since the designed antenna works as a radiator based on a combination of the slot, the microstrip, and the grounds. 2.5×10^2

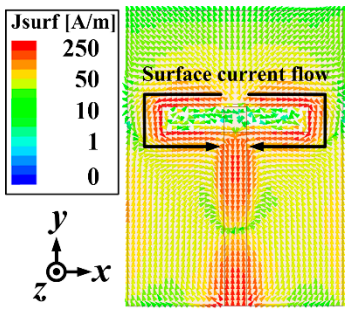

Figure 3. Surface current distribution of slotted aperture at 24.125 GHz.

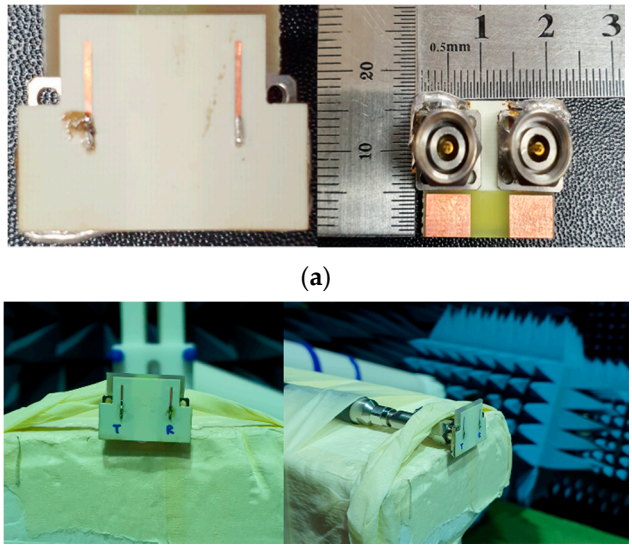

(**a**)

(**b**)

Figure 4. Fabrication and measurement setup of slot-type Doppler radar antenna: (**a**) fabrication; (**b**) measurement setup.

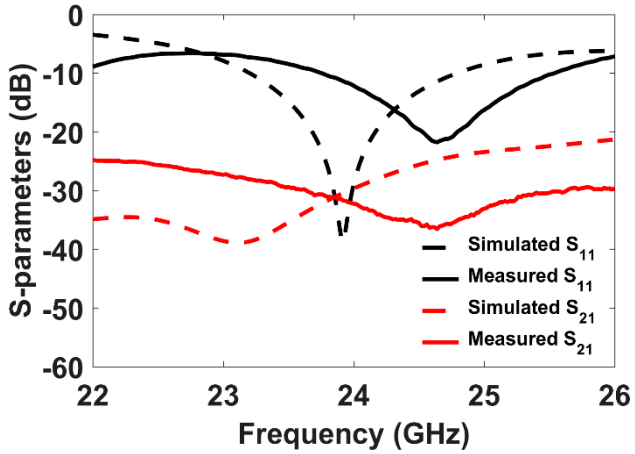

Figure 5. Simulated and measured S-parameters.

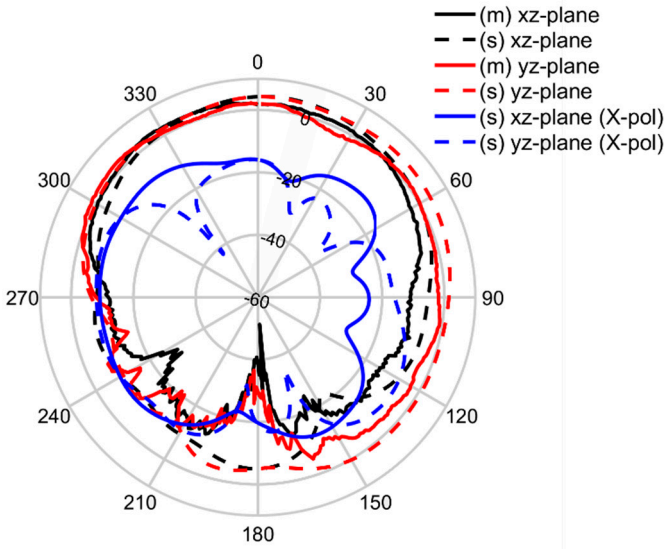

Figure 6. Simulated and measured radiation patterns at 24.125 GHz.

3. Feasible Study of Doppler Radar Antenna for Respiration

In general, quadrature receiver systems are widely used in Doppler radar to detect vital signs, because the performance of single-channel receivers is limited [21]. Two orthogonal output signals of the quadrature receiver system can measure relative phase information. The two signals are represented as the in-phase (I) channel and the quadrature-phase (Q) channel. The magnitude and phase of the I-and Q-channel signals can be displayed via the I/Q plot. Note that the time-varying phase shift is linearly proportional to the displacement caused by human body surface movement. Displacement can be obtained by applying arctangent demodulation to the I and Q signals ratio [22]. Note that we assume that RF and baseband systems are perfect since we focus on the feasibility study of a near-field Doppler radar in terms of antennas and propagation.

As a proof of concept, in this work, we consider human respiration. Toward this purpose, let us assume that the Doppler radar antenna is embedded in the ID badge holder. The designed Doppler radar antenna is placed in front of the abdomen of Duke phantom in Sim4life. The dielectric properties of human tissues can be found in [23]. The distance between the Doppler radar antenna and the human body is changed from 5 to 15 mm because respiration is accompanied by movement of the upper body surface and its movement is usually about 10 mm [24,25]. Figure 7 shows a simulation setup of the designed Doppler radar antenna with Duke phantom in Sim4life. The pulse signal is excited to analyze the frequency response of the designed Doppler radar with the Duke phantom. The total time

spent on simulation is about 5 h by using a DELL T7910 workstation with an NVIDA Tesla K40 GPU accelerator. Figure 8 shows the simulated reflection coefficients. It is observed that that the designed Doppler radar antenna placed at a distance of 5 mm has a reflection coefficient of −9.2 dB and the rest is less than −10 dB at 24.125 GHz.

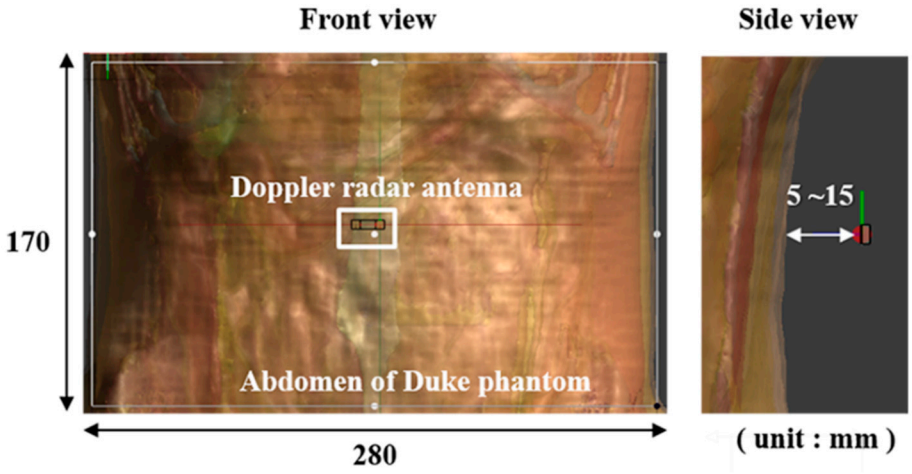

Figure 7. Simulation setup of the designed Doppler radar antenna with Duke phantom in Sim4life.

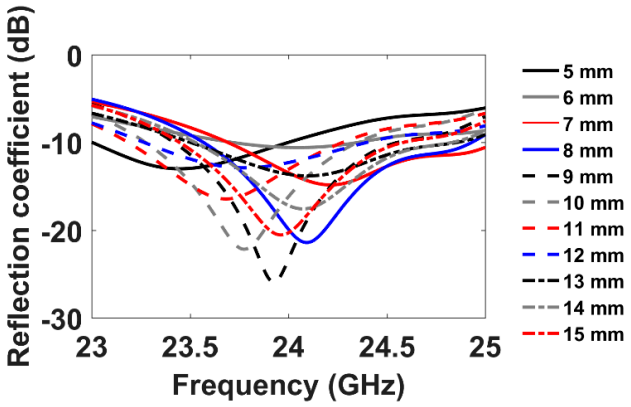

Figure 8. Simulated reflection coefficient of the designed Doppler radar antenna with Duke phantom.

In order to accurately analyze the phase information by the Doppler effect, the direct signal from the transmitter must be excluded from the signal received at the receiver. Note that the direct signals can be subtracted from the received signals by the calibration in the actual Doppler radar system. Before proceeding with the Doppler performance, it is worthy to investigate the antenna fidelity factor and the system fidelity factor [26,27]. The fidelity factors can be obtained as follows:

$$T_N(t) = \frac{T(t)}{\left[\int_{-\infty}^{\infty} |T(t)|^2 dt\right]^{1/2}} \quad (1)$$

$$R_N(t) = \frac{R(t)}{\left[\int_{-\infty}^{\infty} |R(t)|^2 dt\right]^{1/2}} \quad (2)$$

$$F = \max \int_{-\infty}^{\infty} T_N(t) R_N(t+\tau) dt \quad (3)$$

The $T_N(t)$ and $R_N(t)$ are the normalized pulses to compare the shape between the two pulses. The fidelity factor F is the maximum value of the correlation between the normalized pulses. The antenna

fidelity factor is obtained by calculating with the cross-correlation of the radiated E- field and the input signal. As shown in Figure 9a, the good antenna fidelity factor is observed for all angles. The system-fidelity factor is calculated by the cross-correlation between the transmitted pulse and the received pulse. Figure 9b shows the correlation between the transmitted pulse signal and the received pulse signal at the distance of 11 mm. As shown in the Figure 9b, the maximum value of the correlation is almost one and thus the very high system fidelity is expected. Figure 9c shows the system fidelity versus the distance. The results show that the system fidelity factors are very good at all distances and thus the designed slot-type antenna is suitable for Doppler radar applications.

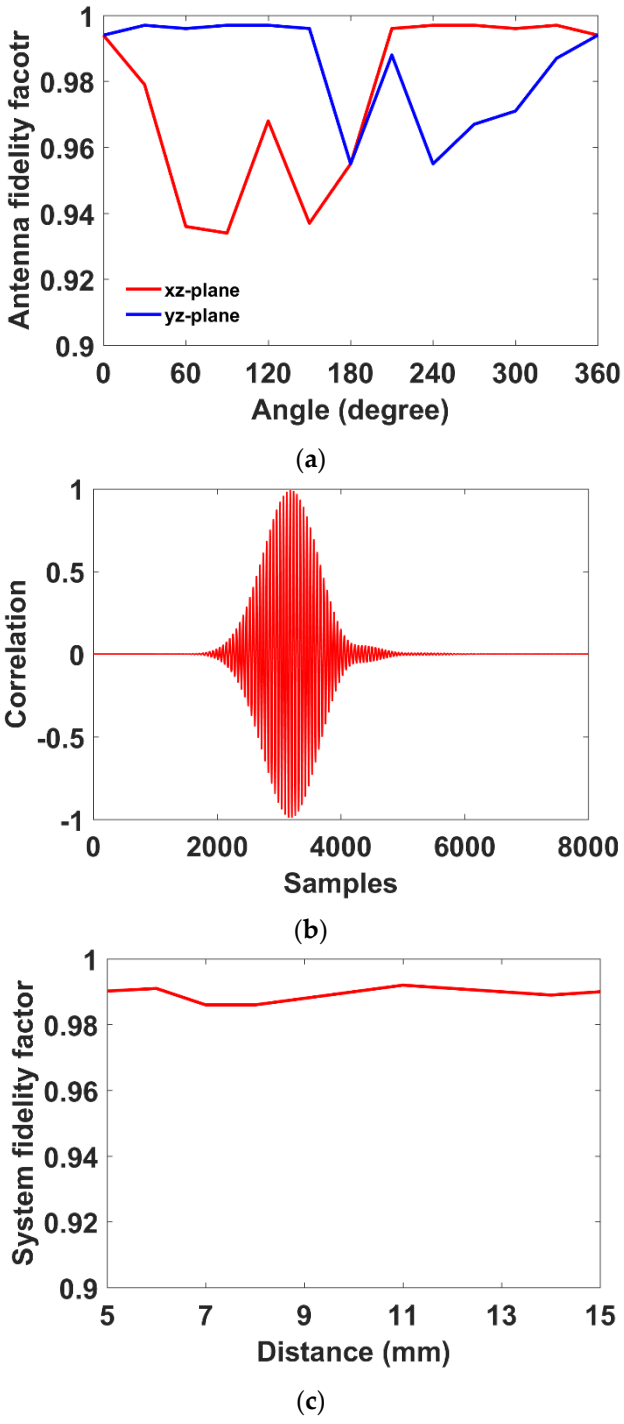

Figure 9. Fidelity factor: (**a**) antenna fidelity factor; (**b**) correlation between Tx pulse and Rx pulse at the distance of 11 mm; (**c**) system fidelity factor.

Next, we plot the amplitude and phase of the signal returned from the phantom over a distance of 5 to 15 mm at 24.125 GHz in Figure 10. The phase of the returned signal is almost linear, and a displacement of 1 mm corresponds to a phase change of about 0.8 rad. The amplitude of the returned signal fluctuates, since the designed Doppler radar operates in near field. However, human body displacement is only related to the phase information and thus this non-flat amplitude response is not problematic for the Doppler radar. The I/Q data are obtained by mixing the returned signal with the transmitting signal. Figure 11 shows I/Q data corresponding to Figure 10. Although the I/Q trace is not a perfect circle (due to non-flat amplitude response), the phase response is almost linear to displacement, as expected.

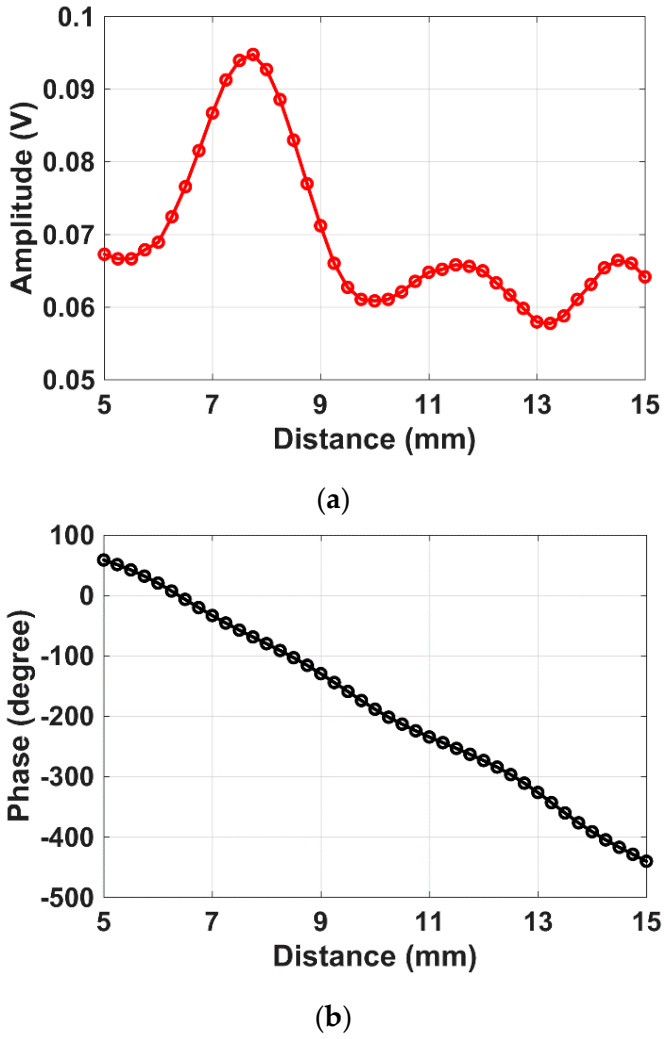

Figure 10. Amplitude and phase of the signal returned from the phantom: (**a**) amplitude; (**b**) phase.

Until now, we analyze the returned signal from the human body in a stationary position. However, the displacement of the human body is not stationary when breathing and thus the time-varying returned signal must be investigated. In this work, to emulate the movement of the human body in breathing, it is assumed that the displacement of the human body changes linearly with time. In specific, the one exhale time is 2 s and the one inhale time is 2 s and thus respiration is periodic to 4 s, as shown in Figure 12. Note that the movement of the human body by actual breathing is complex with respect to time, but the purpose of this work is to investigate the phase-shifted returned signal and thus this linear assumption is appropriate for this work.

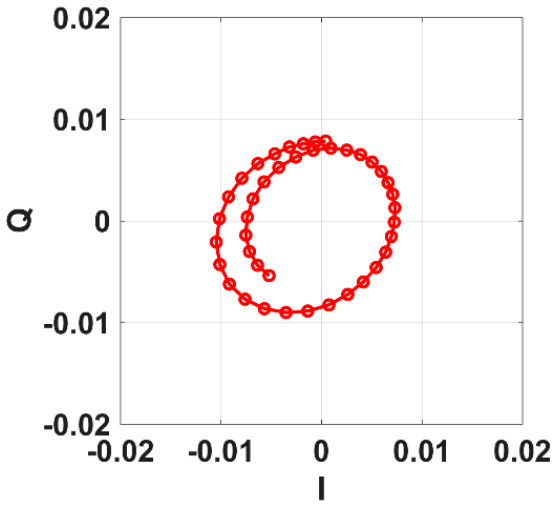

Figure 11. I/Q plot.

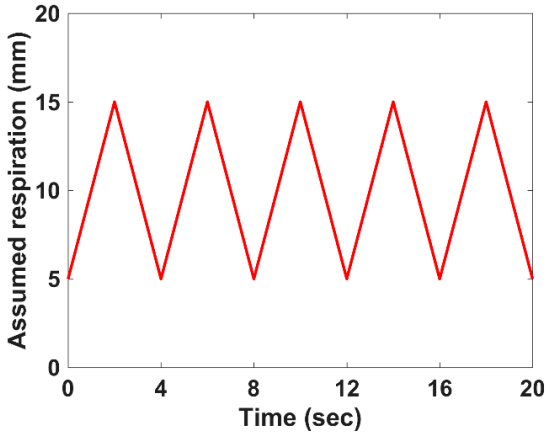

Figure 12. Assumed respiration versus time.

Figure 13a shows the I/Q data for the time-varying returned signal and it is observed that the period of I/Q data is 4 s, same as respiration. Next, the converted displacement is calculated by arctangent demodulation. Ideally, the converted displacement of 0 mm (10 mm) corresponds to the distance between the antenna and the object of 5 mm (15 mm). According to Figure 13b, the converted displacement is 0 mm to 9 mm. Note that the difference between maximum and minimum converted displacement (9 mm) is not the same as human body movement (10 mm) since the abdomen of the phantom is not flat and the human body is not perfectly electric conductor (PEC). We also calculate theoretically the converted displacement of a flat PEC in far field. As shown in the Figure 13, the converted displacement in this case is exactly the same as the movement of the human body. It should be noted that the respiration rate is successfully obtained by the near-field Doppler radar, albeit with little discrepancy of displacement. Numerical experiments show that the designed Doppler radar antenna can sense human respiration in near field in electromagnetic aspects.

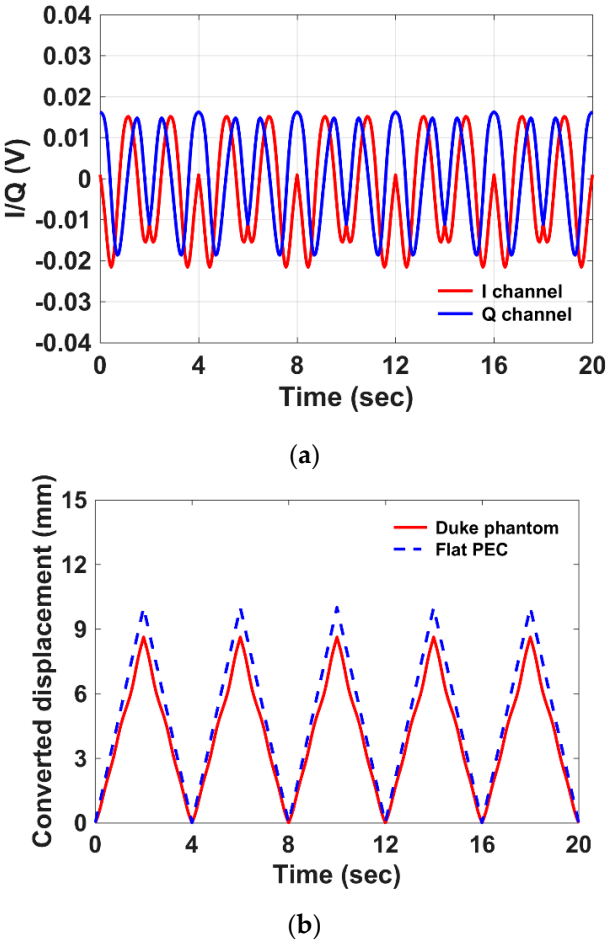

Figure 13. Time-varying I/Q data and arctangent demodulated signals: (**a**) I/Q data for time-varying returned signals; (**b**) converted displacement by arctangent demodulation.

4. Conclusions

In this paper, a feasibility study of the 24 GHz ISM-band Doppler radar antenna for near-field sensing of human respiration in electromagnetic aspects is presented. Since the Doppler radar antenna is assumed to be used in wearable devices, it is designed and fabricated as the slot-type antenna that is less affected by human body effects. The designed slot-type Doppler radar antenna is satisfied with −10 dB reflection coefficient at the target frequency band and lower than −30 dB mutual coupling between the transmitter and the receiver. To study the performance of the designed Doppler radar antenna for near-field sensing human respiration, the Doppler radar antenna is placed in front of the Duke phantom's abdomen and it is simulated while the distance between the Duke phantom and the antenna is varied from 5 to 15 mm. It is observed that the phase of the returned signal is linearly proportional to the displacement, and the phase change of the returned signals is about 0.8 rad corresponding to 1 mm of displacement. Moreover, time-varying returned signals are analyzed using I/Q and arctangent demodulation. Numerical examples demonstrate that the designed Doppler radar can successfully sense human respiration in electromagnetic aspects. It should be noted that the Doppler radar for near-field sensing of human vital signs will be practically feasible when the electromagnetic performance as well as the performance of other parameters in RF systems, baseband systems, and signal processing (e.g., to mitigate DC offset or clutter interference) are fully considered.

Author Contributions: The presented work was carried out in collaboration by all authors. S.P. and S.K. performed the simulations; D.K.K., J.C. and K.-Y.J. participated to the conception and the design; S.P. wrote the paper which was edited by all co-authors. All authors have read and agreed to the published version of the manuscript.

Funding: This research was funded by the Electronics and Telecommunications Research Institute grant funded by the Korean government (19ZH1500, Robust Contactless Wearable Radar Technology with Motion Artifact Removal for Easy-to-Wear Vital-sign Sensing Devices).

Conflicts of Interest: The authors declare no conflict of interest.

References

1. Lee, Y.S.; Pathirana, P.N.; Caelli, T.; Evans, R.J. Doppler radar in respiratory monitoring: Detection and analysis. In Proceedings of the 2013 International Conference on Control, Automation and Information Sciences (ICCAIS), Nha Trang, Vietnam, 25–28 November 2013.
2. Huang, M.-C.; Liu, J.J.; Xu, W.; Gu, C.; Li, C.; Sarrafzadeh, M. A Self-Calibrating Radar Sensor System for Measuring Vital Signs. *IEEE Trans. Biomed. Circuits Syst.* **2015**, *10*, 352–363. [CrossRef] [PubMed]
3. Rahman, A.; Lubecke, V.M.; Boric-Lubecke, O.; Prins, J.H.; Sakamoto, T. Doppler Radar Techniques for Accurate Respiration Characterization and Subject Identification. *IEEE J. Emerg. Sel. Top. Circuits Syst.* **2018**, *8*, 350–359. [CrossRef]
4. Tran, V.P.; Al Jumaily, A.; Islam, S. Doppler Radar-Based Non-Contact Health Monitoring for Obstructive Sleep Apnea Diagnosis: A Comprehensive Review. *Big Data Cogn. Comput.* **2019**, *3*, 3. [CrossRef]
5. Wang, C.; Ellis, J.D. Dynamic Doppler Frequency Shift Errors: Measurement, Characterization, and Compensation. *IEEE Trans. Instrum. Meas.* **2015**, *64*, 1. [CrossRef]
6. Li, C.; Lubecke, V.M.; Boric-Lubecke, O.; Lin, J. A Review on Recent Advances in Doppler Radar Sensors for Noncontact Healthcare Monitoring. *IEEE Trans. Microw. Theory Tech.* **2013**, *61*, 2046–2060. [CrossRef]
7. Zhang, J.; Yang, M.; Zheng, S.; Sun, X. A low-cost Doppler radar system with 24 GHz PLL for remote detection of heart beat. *Microw. Opt. Technol. Lett.* **2008**, *50*, 3139–3142. [CrossRef]
8. Hsu, T.-W.; Tseng, C.-H. Compact 24-GHz Doppler radar module for non-contact human vital-sign detection. In Proceedings of the 2016 International Symposium on Antennas and Propagation (ISAP), Okinawa, Japan, 24–28 October 2016.
9. Girão, P.S.; Postolache, O.; Ramos, P.M.; Pereira, J.M.D.; Postolache, O.A. Microwave Doppler radar in unobtrusive health monitoring. *J. Phys. Conf. Ser.* **2015**, *588*, 012046. [CrossRef]
10. Kagawa, M.; Ueki, K.; Tojima, H.; Matsui, T. Noncontact screening system with two microwave radars for the diagnosis of sleep apnea-hypopnea syndrome. In Proceedings of the 2013 35th Annual International Conference of the IEEE Engineering in Medicine and Biology Society (EMBC), Osaka, Japan, 26 September 2013.
11. Kim, S.; Kim, D.K.; Kim, Y.; Choi, J.; Jung, K.-Y. A 24 GHz ISM-Band Doppler Radar Antenna With High Isolation Characteristic for Moving Target Sensing Applications. *IEEE Antennas Wirel. Propag. Lett.* **2019**, *18*, 1532–1536. [CrossRef]
12. Yang, F.-M.; Peng, L.; Liao, X.; Mo, K.-S.; Jiang, X.; Li, S.M. Coupling Reduction for a Wideband Circularly Polarized Conformal Array Antenna with a Single-Negative Structure. *IEEE Antennas Wirel. Propag. Lett.* **2019**, *18*, 991–995. [CrossRef]
13. Makinen, R.M.; Kellomaki, T. Body Effects on Thin Single-Layer Slot, Self-Complementary, and Wire Antennas. *IEEE Trans. Antennas Propag.* **2013**, *62*, 385–392. [CrossRef]
14. Christ, A.; Kainz, W.; Hahn, E.G.; Honegger, K.; Zefferer, M.; Neufeld, E.; Rascher, W.; Janka, R.; Bautz, W.; Chen, J.; et al. The Virtual Family—Development of surface-based anatomical models of two adults and two children for dosimetric simulations. *Phys. Med. Biol.* **2009**, *55*, N23–N38. [CrossRef] [PubMed]
15. *Sim4life, V5.0.*; Zurich Med. Tech.: Zürich, Switzerland, 2019; Available online: https://zmt.swiss/ (accessed on 1 September 2020).
16. Jung, K.; Ju, S.; Teixeira, F.L. Application of the Modal CFS-PML-FDTD to the Analysis of Magnetic Photonic Crystal Waveguides. *IEEE Microw. Wirel. Components Lett.* **2011**, *21*, 179–181. [CrossRef]
17. Ha, S.-G.; Cho, J.; Lee, J.; Min, B.-W.; Choi, J.; Jung, K.-Y. Numerical Study of Estimating the Arrival Time of UHF Signals for Partial Discharge Localization in a Power Transformer. *J. Electromagn. Eng. Sci.* **2018**, *18*, 94–100. [CrossRef]
18. Kweon, J.-H.; Cho, J.; Park, M.-S.; Jung, K.-Y. FDTD analysis of electromagnetic wave propagation in inhomogeneous ionosphere. *J. Electromagn. Eng. Sci.* **2018**, *18*, 212–214. [CrossRef]
19. Keum, K.; Piao, H.; Choi, J. Design of a Short/Open-Ended Slot Antenna with Capacitive Coupling Feed Strips for Hepta-Band Mobile Application. *J. Electromagn. Eng. Sci.* **2018**, *18*, 46–51. [CrossRef]

20. Balanis, C.A. *Antenna Theory: Analysis and Design*, 4th ed.; John Wiley & Sons, Inc.: New Jersey, NJ, USA, 2005; pp. 639–709.
21. Park, B.K.; Yamada, S.; Boric-Lubecke, O.; Lubecke, V. Single-channel receiver limitations in doppler radar measurements of periodic motion. In Proceedings of the 2006 IEEE Radio and Wireless Symposium, San Diego, CA, USA, 17–19 January 2006.
22. Boric-Lubecke, O.; Lubecke, V.; Droitcour, A.D.; Park, B.-K.; Singh, A. *Doppler Radar Physiological Sensing*, 1st ed.; John Wiley & Sons: Hoboken, NJ, USA, 2013.
23. Parametric Model for the Calculation of the Dielectric Properties of Body Tissues in the Frequency Range 10 Hz-100 GHz. Available online: http://niremf.ifac.cnr.it/tissprop/ (accessed on 1 May 2020).
24. Kaneko, H.; Horie, J. Breathing movements of the chest and abdominal wall in healthy subjects. *Respir. Care* **2012**, *57*, 1442–1451. [CrossRef] [PubMed]
25. Harauz, G.; Bronskill, M.J. Comparison of the liver's respiratory motion in the supine and upright positions: Concise communication. *J. Nucl. Med* **1979**, *20*, 733–735.
26. Quintero, G.; Zurcher, J.-F.; Skrivervik, A.K. System fidelity factor: A new method for comparing UWB antennas. *IEEE Trans. Antennas Propag.* **2011**, *59*, 2502–2512.
27. Kwon, D.-H. Effect of Antenna Gain and Group Delay Variations on Pulse-Preserving Capabilities of Ultrawideband Antennas. *IEEE Trans. Antennas Propag.* **2006**, *54*, 2208–2215. [CrossRef]